Metallomics

Accepted Manuscript

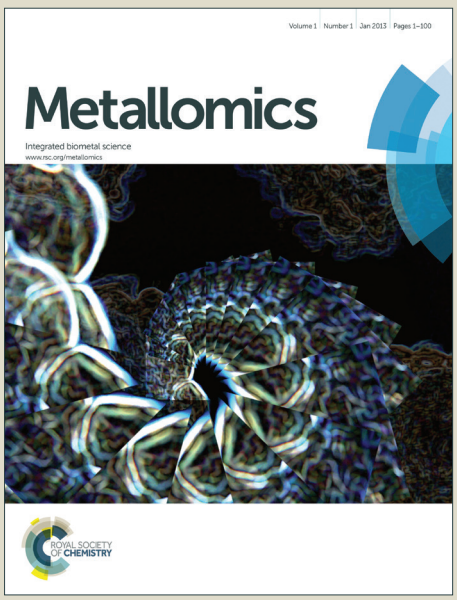

ROYAL SOCIETY OF CHEMISTRY

www.rsc.org/metallomics

Structural, Spectroscopic and Functional Investigation into Fe-substituted MnSOD from Human Pathogen *Clostridium difficile*

Wei Li[1], *Hongfei Wang*[2], *Qingli Wang*[3] *and Xiangshi Tan*[1]*

[1]Department of Chemistry & Institutes of Biomedical Sciences, Fudan University, Shanghai 200433, China.

[2]Institute of Molecular Science, Shanxi University, Taiyuan 030006, China

[3]College of Chemistry, Chemical Engineering and Materials Science, Shandong Normal University, Jinan 250014, China

*To whom correspondence should be addressed. Email: xstan@fudan.edu.cn

Phone: +86 -21-55664475. Fax: + 86-21-65641740

Abstract

Clostridium difficile， which inhabits the human digestive tract, is an etiological agent that causes pseudomembranous colitis and antibiotic-associated diarrhea. The oxidative stress tightly relates to its virulence, which highlights the function of its superoxide dismutase (SOD). The SOD from *Clostridium difficile* (SOD_{cd}) is a Mn/Fe cambialistic SOD with $MnSOD_{cd}$ exhibiting an optimal activity while Fe-sub-$MnSOD_{cd}$ showing 10-fold less activity. To explain why the Fe-loaded protein exhibits a much lower activity than the Mn-loaded form, Fe-sub-$MnSOD_{cd}$ and $MnSOD_{cd}$ were expressed in *E. coli* using M9 minimal medium, and characterized by X-ray crystallography, metal analysis, optical and EPR pH titration, azide binding affinity, *etc.* The pK_a values for the active site residues and substrate affinities determined by spectroscopic titrations indicated that $MnSOD_{cd}$ has a higher affinity with substrate compared to Fe-sub-$MnSOD_{cd}$, while Fe-sub-$MnSOD_{cd}$ has more affinity for OH^-. The different tendency of the anion ligation may be ascribed to the electronic configurations of Fe^{3+} in d^5 *vs* Mn^{3+} in d^4, and it could be tuned by the hydrogen-bonding network around the active site of SOD_{cd}. Furthermore, the free energy for the $O_2^{\cdot-}$ oxidation-reduction transition state from DFT calculation, demonstrated that $MnSOD_{cd}$ could disproportionate $O_2^{\cdot-}$ more easily than Fe-sub-$MnSOD_{cd}$. These results revealed that SOD_{cd} could exquisitely differentiate between the Mn- and Fe-based activity. This metal specificity for SOD_{cd} may benefit the pathogenicity of *C. difficile* and pave a fundamental way for retarding *C. difficile* associated diseases.

Keywords: Fe-sub-MnSOD, MnSOD, Crystal structure, EPR, *Clostridium difficile*

Introduction

Clostridium difficile is an anaerobic gram-positive spore-forming pathogen bacillus, which infects human through the fecal-oral route, adheres to human gastrointestinal tract，and causes an acute illness called *Clostridium difficile* infection (CDI) such as severe diarrhea, antibiotic-associated colitis, pseudomembranous colitis, toxic megacolon, and intestinal perforations[1]. The virulent surface proteins, toxin A and toxin B，are demonstrated to induce mitochondrial swelling and release of reactive oxygen species (ROS) in its germination process[1, 2]. On the other hand, the internalization of toxin A into host cells could elicit severe inflammatory cascade and produce substantial ROS, which deeply attacks the host cells and facilitate the infection of *C. difficile*[3]. However, this infiltration process would put this pathogenic bacterium in the oxidative tension, which is exacerbated by the tremendous oxidative byproducts of the oxidative phosphorylation and tricarboxylic acid cycles (such as oxidation of flavoproteins) occurring in human digestive tract[4]. To cope with the oxidative stress, *C. difficile* has evolved a highly effective superoxide dismutase SOD_{cd} to detoxify ROS[5].

SOD_{cd} catalyzes the disproportionation of superoxide anion with a two-step ping-pong mechanism，in which the metal ion cycles between the reductive and oxidative states (eq. 1 and 2)[6]. Fe, Mn, Cu/Zn, or Ni ion has been evolved as SOD cofactor, respectively. FeSOD and MnSOD are two very similar members of the SOD

family[7] and they have no significant similarity with the Cu/Zn- , or Ni-containing SODs[8]. FeSOD and MnSOD share highly similar amino acid sequence with highly identical protein folding, as well as virtually same active site coordination shell[9]. In both cases, the metal ion is coordinated in a trigonal bipyramidal geometry with two histidines and one aspartate in the equatorial plane, while the third histidine residue and a coordinated solvent as axial ligands. The coordinated solvent is involved in a hydrogen-bonding network linked by Gln178 and Tyr64 residues (named according to the sequence of *C. difficile*) **(Fig. 1)**.

$$M^{n+}E + O_2^{\cdot-} + H^+ \rightarrow M^{(n-1)+}E_H^{+} + O_2 \qquad (1a)$$

$$M^{(n-1)+}E_H^{+} + O_2^{\cdot-} + H^+ \rightarrow M^{n+}E + H_2O_2 \qquad (1b)$$

$$2\ O_2^{\cdot-} + 2\ H^+ \rightarrow O_2 + H_2O_2 \qquad (2)$$

Despite the extraordinarily structural similarity of Fe- and MnSOD, they differ subtly regarding to the following aspects: (1) Mn^{2+}SOD could bind H_2O_2 and form an unproductive intermediate presumed to be a side-on Mn^{3+}-peroxo complex, from which it exhibits product inhibition effect[10,11]. FeSOD is irreversibly inactivated by HO_2^- with concomitant Fe release and amino acid modification[10]. (2) The active center of MnSOD is more intimately coupled to the rest of the protein (Tyr64) than that of FeSOD, which is reflected by MnSOD's higher affinity towards substrate or its analogues, reminiscent of the more elaborate structure for MnSOD in the evolution progress from more primitive FeSOD[11]. (3) The matrix of MnSOD could depress the reduction midpoint potential (E_m) of the bound metal ion more than that for FeSOD[12]. (4) Fe- and MnSOD showed distinct active-site pK_a, which tightly relate to their

catalytic ability since two protons are required for a turnover[13] (eq. 1 and 2). Although these originate in bulk solvent, they are almost certainly supplied to substrate and/or nascent product by active site residues, including the existing coordinated solvent molecule as one proton source[14] and Tyr64 as the other[15]. Much effort has been dedicated into accurately determining the active site pK_as. Fe^{3+}SOD from *E. coli* has a pK_a of 8.5-9.0[16, 17], assigned to a hydroxide ion to the five-coordinate active site based on the fact that the K_m increased with the raised pH due to the competition inhibition of OH^-[18]. Another evidence came from the crystal structure of *Propionibacterium shermanii* Fe^{3+}SOD under pH 8.5, showing a OH^- as the sixth ligand for Fe^{3+} [19]. By comparison, the *pKa* of Fe^{2+}SOD was associated with the deprotonation of Tyr64 based on the site-directed mutation studies by NMR[20]. Comparatively, Mn^{3+}SOD and Mn^{2+}SOD have active site *pKa*s of 9.5 and 10.5, respectively, which were associated with the depronation of Tyr64 based on optical[21] and EPR titrations[11].

Given the existence of those differences, most of the Fe- and MnSODs exhibit strictly metal ion specificity and reactivity, i.e., Fe incorporated into the MnSOD protein scaffold [Fe(Mn)SOD][22] or Mn incorporated into the FeSOD [Mn(Fe)SOD][23] is catalytically inactive due to the improper substrate binding affinity or redox potential. However, besides the Mn and Fe specific SOD, there exists a group of cambialistic SODs exhibiting substantial activities whenever Mn or Fe occupied[24]. It seems that cambialistic Fe/MnSOD group might represents an intermediate in the evolution process from the anaerobic FeSOD to aerobic MnSOD accompanying the terrestrial atmosphere oxygen formation[25, 26]. Cambialistic SOD of microorganism

could bind either Mn or Fe based on their growth conditions[27]. Generally, cambialistic SODs prefer Mn to Fe in aerobic, Mn efficient, and high pH environments[28]. The flexibility of cambialistic SOD utilizing either Mn or Fe ion as its cofactor according to the contingent growth conditions could encourage microorganisms to fluctuate between aerobic and anaerobic environment and to accommodate the concomitant changes in metal availability[29].

The Fe ion affinity of SOD_{cd} is tighter than Mn ion, when expressed aerobically in *E. coli*, while the MnSOD displays about 10-fold more activity than the Fe-form[5], indicating that the SOD_{cd} is a kind of MnSOD with some cambialistic character. The cambialistic character of $MnSOD_{cd}$ might facilitate *C. difficile* survive in the complicated human digestive tract with various oxygen concentrations and metals distributions in stomach, gut, bile, and intestine[30, 31]. To explain why the $MnSOD_{cd}$ exhibits 10 times higher activity than the Fe-form and the mechanistic differences between the Fe- and Mn-dependent SOD_{cd} , the Fe-sub-$MnSOD_{cd}$ and $MnSOD_{cd}$ were expressed in *E. coli* using metal supplement M9 medium, and the structure-function-reactivity relationships of Fe-sub-$MnSOD_{cd}$ and $MnSOD_{cd}$ were explored using spectroscopic, crystallographic and DFT computational methods . The SOD activity assay showed that Fe-sub-$MnSOD_{cd}$ was more vulnerable to OH^- and H_2O_2 inhibition while less sensitive to azide than $MnSOD_{cd}$. The active site pK_a*s* of Fe-sub-$MnSOD_{cd}$ and $MnSOD_{cd}$ revealed by spectroscopic titrations indicated that $MnSOD_{cd}$ has a higher affinity with substrate than Fe-sub-$MnSOD_{cd}$, while Fe-sub-$MnSOD_{cd}$ prefers OH^- to the substrate. Furthermore, systematic DFT

calculations were performed to identify possible intermediates to be mediated in the reaction cycles of Fe- and $MnSOD_{cd}$, from which the free energies were obtained to explain the lower activity of Fe-sub-$MnSOD_{cd}$. These results provide new insights into the molecular mechanism for the same SOD_{cd} moiety to exhibit distinct function when occupied by similar Mn or Fe ion.

Experiments and materials

Preparation and characterization of Fe-sub-$MnSOD_{cd}$

Fe-sub-$MnSOD_{cd}$ and $MnSOD_{cd}$ were expressed in *E. coli* using M9 minimal medium (1×M9 salts, 2 mM $MgSO_4$, 0.1 mM $CaCl_2$, 0.00005% thiamine and 0.4% glucose). When the OD reached to 0.5, 1mM $FeCl_3$/or $MnCl_2$ was added into the M9 medium and the protein expression was introduced with 0.5 mM IPTG overnight. The protein was purified as what reported previously[5]. The protein concentration was determined by Bradford method[32]. The metal contents were analyzed by ICP-AES (Inductively Coupled Plasma-Atomic Emission Spectroscopy) on Zeeman atomic absorption spectrometer (Z-5000, Hitachi, Japan). Iron standard solution was purchased from *Merck Labs*. Electronic absorption spectra were recorded on a HP8453 UV–Visible spectrophotometer (*Agilent)*. X-band EPR spectra were recorded at 4 K on a Bruker EMX 300 equipped with an Oxford 900 cytostat. The spectra were recorded under the following conditions: microwave frequency, 9.44 GHz; microwave power, 2.0 mW; modulation frequency, 100 kHz; modulation amplitude, 4.00 G; and time constant, 163.84 ms. The SOD samples (0.5 mM) were buffered in 50 mM

potassium phosphate, pH 7.8 plus 10% glycerol. N_3^--Fe-sub-$MnSOD_{cd}$ was prepared by adding excessive NaN_3 into the Fe-sub-$MnSOD_{cd}$ and then incubating for a few hours.

SOD activity

SOD activity was assayed according to McCord and Fridovich's protocol[5, 33]. For azide and hydrogen peroxide inhibition, aliquots of the inhibitors were added into the reaction solution, and the reduction curves were recorded. For clarifying the pH dependence of SOD_{cd} activity, the reaction cocktail pH values were adjusted by HCl and NaOH titrations.

Optical, EPR pH titration and Azide binding

Optical pH titrations for $MnSOD_{cd}$ and Fe-sub-$MnSOD_{cd}$ were performed using Hewlett-Packard 8453 spectrophotometer. pH values were measured continuously using a combination pH microelectrode (Microelectrodes Inc.). The pH value was increased in a small step by adding 100 mM KOH and then the optical spectrum was recorded at each pH value. *pK* value was obtained by fitting the data with the Henderson-Hasselbalch equation $(A_A-A_{obs})/(A_A-A_B) = (K)/(K+10^{-(pH)})$, where A_A and A_B (as the acid and base forms) are absorbance values at 476 nm, respectively. A_{obs} is the observed absorbance at a given pH value, K is the acid dissociation constant and the Hill coefficient is set to 1. The EPR pH titration was performed as follows: The pH values of Fe-sub-$MnSOD_{cd}$ were adjusted successively with 100 mM KOH. The SOD_{cd} sample at each pH point, measured using a microelectrode, was transferred into an EPR tube and promptly frozen in liquid nitrogen. Signal amplitudes in the

spectra were plotted as a function of pH values. The pK_a values were evaluated by fitting with the Henderson-Hasselbalch equation neglecting cooperativity.

Azide binding affinity of these SOD_{cd} proteins was determined by titration of azide to the different SOD_{cd} proteins, respectively, using Hewlett-Packard8453 spectrophotometer at 25℃. The apparent dissociation constant of azide for each SOD_{cd} protein was obtained by fitting the absorbance data to the following eq (1), which describes weak binding with an invariant absorbance background B and addition absorbance A_{max} when SOD protein saturated with azide.

$$A([S])= A_{max}* [S]/(K_d' + [S]) + B \quad (1)$$

The apparent K_d was corrected for the pK (4.7) of N_3H based on the equilibrium ($N_3H \rightarrow H^+ + N_3^-$) using eq (2), generating the azide dissociation constant K_d'.

$$K_d' = (1+10^{(pH-pK)})K_d \quad (2)$$

Crystallography

Azide-Fe-sub-$MnSOD_{cd}$ (~20 mg/ml) was crystallized by hanging-drop vapor diffusion method at 16°C under the following conditions: 60% v/v tacsimate™ at pH 7.0. The flash-cooled SOD_{cd} crystals were then mounted under a liquid N_2 stream, and diffraction data were collected from single crystals on beamline BLXU17 at Shanghai Synchrotron Facility (SSRF) of China, using a ADSC QUANTUM 315 detector with wavelength of 0.9792 Å at 100K. The diffraction data were processed and scaled with HKL-2000[34]. The structures were solved by the molecular replacement method and the 1.6 Å structure of *Bacillus subtilis* SOD (PDB code 2RCV)[35] was used as the

starting model. Manual adjustment of the model was carried out using the program COOT[36] and the model was refined by Refmac5[37] and PHENIX[38]. Stereochemical quality of the structure was checked by using PROCHECK[39]. All the data collection and refinement statistics were listed in **Table 1**. The structure has been deposited in the Protein Data Bank (PDB), with the accession code 4JYY. Structural figures were prepared using PyMOL[40].

DFT calculations

From the crystal structures of $MnSOD_{cd}$ (4JZG) and Fe-sub-$MnSOD_{cd}$ (3TJT), the metal clusters and the additional second-sphere residues Tyr64 and Gln178 were extracted. In all cases, the amino-acid residues were truncated at their Cα atoms by replacing the adjacent backbone atoms with H atoms. The His and Asp ligands were modeled by imidazole and acetate ions, whereas the Gln146 and Tyr64 by an acetamide and tyrosinate ions, respectively **(ESI)**. The terminal methyl of the ligands (including His56, His111, His197 and Asp193), and the terminal methyl of Gln178 and Tyr64, were restrained when the geometries optimizations were performed **(Table S1 and Fig. S2)**. We used $O_2^{-\cdot}$ conjugated acid form [hydroperoxyl radical ($^{\cdot}$OOH)] in place of superoxide ($O_2^{\cdot-}$) as the reactant[37-39]. The configurations of the reaction reactants, products and transition states were also attained **(Table S2 and Fig. S3).** All calculations were carried out with the GAUSSIAN 03 software package[41]. All geometries were fully optimized in a vacuum with the hybrid density functional theory (DFT) at the B3LYP/6-31G(d, p) level, except for iron and manganese atoms, which were optimized with the B3LYP/6-31G(2d, p) method[41-42].

Vibrational frequencies are analytically computed at the same level in order to confirm that a local minimum has no imaginary frequency. Zero-point energies and thermal corrections to the Gibbs free energy (at 298 K and 1 atm pressure, using an ideal-gas approximation[42]) were calculated from the frequency calculation, obtained with the same method as for the geometry optimizations. The binding free energies of the ·OOH to the metal sites were corrected by a constant of -32 kJ/mol, representing the difference in the estimated translational entropy from the Sackur–Tetrode equation[43]. When considering the energy change associated with protonation of $O_2^{\cdot-}$, a correction of -3.0 kcal/mol is further added to the energy of the states involved by ·OOH to reference them to the true reactants ($O_2^{\cdot-}$ + H^+)[44]. Their catalytic potencies were primarily studied by comparing the energy gaps between HOMOs and LUMOs in Fe/MnSOD$_{cd}$/$O_2^{\cdot-}$ according to the frontier molecular orbital (FMO) theory **(Fig. S4)**[45]. Furthermore, the feasibility to dismutate superoxide for MnSOD$_{cd}$ and Fe-sub-MnSOD$_{cd}$ were also investigated by comparing their transition states free energies and their $O_2^{\cdot-}$ disproportionation reaction ΔGs.

Results

Preparation and characterization of Fe-sub-MnSOD$_{cd}$

The Fe-sub-MnSOD$_{cd}$ could be obtained by denaturing the isolated protein, extracting the miscellaneous metals and refolding in presence of the designed metal[5]. But the low metal occupancy of the SOD$_{cd}$ reflected the low efficiency for the *in vitro* metal insertion. The metal uptake for Mn/FeSOD requires activation energy to unfold

the protein peptide [46, 47]. *In vivo*, the metallation of SOD was probably under the aid of chaperone protein[48]. In this study, we alternatively prepared Fe-sub-SOD_{cd} by virtue of M9 minimal medium. The ICP-AES result showed that the metal occupancy was 0.82 in Fe-sub-SOD_{cd}. The gel filtration profiles and CD spectra indicated that Fe-sub-$MnSOD_{cd}$ had identical gross assembly and the second structure with $MnSOD_{cd}$.

The Fe-sub-$MnSOD_{cd}$ was characterized by UV/Vis and EPR spectra, which showed a shoulder absorption at 340 nm as the characteristic of Fe-specific SOD[50,51], ascribed to the LMCT transition bands between Fe^{3+} and the coordinated Asp oxygen. The intensity of this shoulder increased as azide was added, which could be assigned to the charge transfer between azide group and Fe^{3+} center **(Fig. 2)**. Interestingly, the molar extinction coefficient of Fe-sub-$MnSOD_{cd}$ is much lower (300 $M^{-1}cm^{-1}$) than that (1270 $M^{-1}cm^{-1}$) of the *P. ovalis* Fe-specific SOD[49], which reflects that the absorbance spectrum of Fe-sub-$MnSOD_{cd}$ intervenes between those of Fe-specific SOD and Fe-sub-Mn-specific SOD. The result thus indicated the minor cambialistic character of SOD_{cd}. The EPR spectrum **(Fig. 2)** of Fe-sub-$MnSOD_{cd}$ exhibited an dominated Fe(III) species, and the features near 1,570 G ($g \approx 4.3$) are characteristic of high spin (S = 5/2 ferric iron in a strongly rhombic environment)[50]. Further, the g =9.32 resonance was associated with the low-field component requiring inverted zero field splitting of the high spin S =5/2 sextet ground state[51]. At higher field, the transitions arising from the middle Kramers doublet are split (g = 3.51, 3.85 and 4.87), reflecting a low rhombic Fe(III) site in the protein[52]. When azide was added, the

anisotropy signals disappeared and exhibited a strong rhombic symmetry resonance at g=4.31 (rhombic limit, characteristic of an octahedral Fe^{3+} site) along with the notable signal at 9.27 (most likely representing the zero-field splitting, indicating a smaller *D* and more rombic), suggesting that azide coordinated to the Fe^{3+} center forming a six-coordination state[53].

Activities of $MnSOD_{cd}$ and Fe-sub-$MnSOD_{cd}$

$MnSOD_{cd}$ showed ~10-fold higher catalytic activity than Fe-sub-$MnSOD_{cd}$ based on the XO/cyt *c* method. The pH dependent activity profiles **(Fig. 3)** showed that the activity of $MnSOD_{cd}$ was not obviously effected by pH ranging from 5.5 to 11.0 (although minor decrease at the higher pH), while the activity of Fe-sub-$MnSOD_{cd}$ was pH dependent with a transition at about pH 7.6. The pH relatively independent activity of $MnSOD_{cd}$ could render SOD_{cd} working more smoothly in human digestive tract. To evaluate the effect of H_2O_2 on SOD_{cd} activity, the activities of $MnSOD_{cd}$ and Fe-sub-$MnSOD_{cd}$ were measured in presence of different concentrations of H_2O_2. The results showed that $MnSOD_{cd}$ was less sensitive to H_2O_2 inhibition than Fe-sub-$MnSOD_{cd}$ **(Fig. 3)**. MnSOD family was demonstrated to accommodate H_2O_2 by the formation of side on peroxo-Mn intermediate and exhibit product inhibition effect[11]. By contrast, the conformations of several Trp residues around the active site make FeSOD more prone to H_2O_2 inactivation. The product inhibition effect of $MnSOD_{cd}$ could avoid excessive H_2O_2 production and may benefit the H_2O_2 homeostasis in *C. difficile*.

Azide was usually used as a competitive inhibitor and substrate analogue for SOD since it is an isoelectronic species to superoxide anion[52]. The azide inhibition experiments **(Fig. 3)** showed that azide could inhibit the activity of $MnSOD_{cd}$ more with the higher azide binding affinity than that of Fe-sub-$MnSOD_{cd}$.

Spectroscopic titrations of $MnSOD_{cd}$ and Fe-sub-$MnSOD_{cd}$

UV/Vis pH titrations of Fe-sub-$MnSOD_{cd}$ exhibited a pK_a of ~7.2, while the $MnSOD_{cd}$ showed a pK_a of ~8.7 **(Fig. 4)**. The EPR pH titration of Fe-sub-$MnSOD_{cd}$ also exhibited a pK_a of 7.5 **(Fig. 5)**. The same p*Ka* value from UV/Vis and EPR titrations for Fe-sub-$MnSOD_{cd}$ indicated that the same event occurred at the Fe center when the buffer pH increased. Here we assigned the p*Ka* to the sixth OH^- ligation to Fe^{3+} center considering the Jahn-Teller stabilization of the d^5 Fe^{3+} center upon the sixth ligand ligation in Fe-sub-$MnSOD_{cd}$[11]. For $Mn^{3+}SOD_{cd}$, the absorbance at ~478 nm declined upon pH increasing, which was not due to the reduction of Mn^{3+} according to the EPR spectra **(Fig. S1)**. Based on the electronic configuration, $Mn^{3+}SOD_{cd}$ would not bind OH^- readily as Fe^{3+}-sub-$MnSOD_{cd}$ and the ionization of Tyr64 could happen first in $Mn^{3+}SOD_{cd}$. Therefore, we ascribed the pK_a of ~8.7 in $MnSOD_{cd}$ to the deprotonation of Tyr64. Interestingly, the pK_a of Fe-sub-$MnSOD_{cd}$ was consistent with its activity behavior (p*Ka* = ~ 7.6), indicating that the exogenous incoming OH^- would impel substrate binding and decrease its SOD activity.

The substrate analogue (azide) titrations showed that $MnSOD_{cd}$ has a K_d of ~6.5 mM, smaller than that of Fe-sub-$MnSOD_{cd}$ (~12.3 mM) **(Fig. 6)**, which was

consistent with the above azide inhibitory experiments and indicated that $MnSOD_{cd}$ has a higher substrate binding affinity than Fe-sub-$MnSOD_{cd}$. Collectively, the spectroscopic titration results revealed that $MnSOD_{cd}$ preferably bound substrate while Fe-sub-$MnSOD_{cd}$ inclined to bind OH^-, which in turn modulates the SOD_{cd} activity.

The crystal structure of azide-Fe-sub-$MnSOD_{cd}$

The crystal structure of N_3^--Fe-sub-$MnSOD_{cd}$ exhibited an orthorhombic form which owned a space group of $P6_522$ with unit cell dimensions of a=80.5 Å, b=80.5 Å, and c= 249.5 Å, in an asymmetric unit. The overall structure was very similar to that of $MnSOD_{cd}$ and Fe-sub-$MnSOD_{cd}$[5]. The Fe active center revealed a similar metal coordination geometry of distorted trigonal bipyramidal formed by His111, His197, Asp193, His56 and a hydroxide or water **(Fig. 7)**. As indicated in **Table 2**, the Fe^{3+}-$O_{coordSolv}$ distance is 2.23 Å, shorter than that of Mn-$O_{coordSolv}$ (2.46 Å), which may stem from the mixture oxidation state (2+/3+) in the crystal structure of $MnSOD_{cd}$.

Unexpectedly, we did not observe the azide electron density in the first coordination sphere although we soaked Fe-sub-$MnSOD_{cd}$ crystal at high concentration azide (200 mM) for a few days. The azide located in the vicinity of substrate channel due to the hindrance by hydrogen bonding with Thr99, Arg102 and Asp91 **(Fig. 7)**. This result was different from that of FeSOD from *E. coli*, where azide bound as a sixth ligand with distorted octahedral geometry[54], but in consistence

with the azide-MnSOD from *E. coli* reported by Whittaker *et al* (PDB: 1ZJZ). These different azide binding modes may result from different crystallization conditions in terms of buffer pH and salt concentration. Possibly, our complex crystal structure may represent an intermediate state in a progress of azide entering into the metal center.

DFT calculations for Fe-sub-MnSOD$_{cd}$ and MnSOD$_{cd}$

The key residues from the first and second coordination sphere were selected to reach to single point energy equilibrium **(ESI).** Firstly, the catalytic competence towards ·OOH was compared according to the frontier molecular orbital (FMO) theory[45]. The computed HOMO/LUMO energy gaps between the first-sphere reactants indicated MnSOD$_{cd}$ potentiated $O_2^{\cdot-}$ disproportionation more easily than Fe-sub-MnSOD$_{cd}$ **(Fig. S4)**. Furthermore, their catalytic potencies were also investigated based on the reaction transition states associated Gibbs free energies, which were illustrated in the **Fig. 8** (including the superoxide oxidation and reduction steps). The whole reaction was an exothermic and spontaneous process. In the first half-reaction, the reaction energy 16.3 kcal/mol for MnSOD$_{cd}$ (12.9 kcal/mol for Fe-sub-MnSOD$_{cd}$) was released; and the second half-reaction gave out ~13.7 kcal/mol for MnSOD$_{cd}$ and 10.1 kcal/mol for Fe-sub-MnSOD$_{cd}$. Thus these energies revealed that both the superoxide oxidation and reduction steps for MnSOD$_{cd}$ are more thermodynamically favorable than the Fe analogue. Besides, the free energies of transition states for MnSOD$_{cd}$ are also lower than those of Fe-sub-MnSOD$_{cd}$, indicating that the reaction barriers for MnSOD$_{cd}$ are lower than that for

Fe-sub-$MnSOD_{cd}$. Thus the DFT energetic calculations demonstrated that $MnSOD_{cd}$ catalyzes $O_2^{\cdot-}$ turnover more easily either from thermodynamic or kinetic respect, which is consistent with the higher activity of $MnSOD_{cd}$.

Discussion

(1) The metal cognate character and the hydrogen-bonding network of the active site

Fe-sub-$MnSOD_{cd}$ exhibited 1/10 SOD activity of $MnSOD_{cd}$[5]. UV/Vis, EPR and azide titration investigations were carried out and the distinct pH dependent events for $MnSOD_{cd}$ and Fe-sub-$MnSOD_{cd}$ were found to dissect the activity difference. The metal cognate character, i.e. the d orbital electronic configuration and ligand field stabilization, could impact its active site p*Ka*. On the other hand, the p*Ka* could be fine-tuned by the conserved hydrogen-bonding network including the existing coordinated solvent, Gln178, Tyr64 and His60 located at the active site, which plays important roles in relaying the liable protons, and reorienting the substrate **(Fig. 1** and **Fig. 7)**[5, 13, 61]. The difference of pK_a stems from metal cognate character and the different distribution of labile proton density in the hydrogen-bonding networks of the SOD_{cd}. Because of the electronic configurations of Mn^{3+} in d^4 *vs* Fe^{3+} in d^5, binding of the sixth ligand to Mn^{3+} costs Jahn-Teller stabilization, whereas gaining Jahn-Teller stabilization when binding of the sixth ligand to Fe^{3+}. Thus we assigned the pK_a of 7.50 for Fe^{3+}-sub-$MnSOD_{cd}$ to the sixth OH^- binding into the inner sphere[13]. The bleaching of the absorption feature at 340 nm reflects the decreased CT transitions

between aspartate and ferric iron upon the sixth OH^- binding. The resulting additional negative charge in the active site adjacent to the substrate access channel would disfavor Tyr64 deprotonation. Indeed, because Fe^{3+}-sub-$MnSOD_{cd}$ began to denature before a high pH asymptote was reached, it is impossible to observe the p*K*a of Tyr64 deprotonation. By contrast, upon pH increasing, $Mn^{3+}SOD_{cd}$ would not bind OH^- as readily as Fe^{3+}-sub-$MnSOD_{cd}$. Alternatively, we noticed that a titrable residue Tyr64 in the proximity of Mn^{3+} (5.4 Å) and Tyr64 ionization would cause a significant change in Mn^{3+}'s local dielectric, which would alter the intensities of electric-dipole-mediated transitions[11]. Thus, the deprotonation of Tyr64 would cause substantial UV/Vis alterations in $Mn^{3+}SOD_{cd}$. Therefore, we ascribed the p*K*a of 8.72 to the deprotonation of Tyr64. The ionization of Tyr64 would lead additional negative charge in the active site to disfavor additional OH^- binding.

As shown in the crystal structure of SOD_{cd}, Gln178 donates stronger hydrogen bond to Tyr64 in $MnSOD_{cd}$ than that in Fe-sub-$MnSOD_{cd}$[5], which would depress the p*K*a of Tyr64. Thus Tyr64 deprotonates prior to OH^- binds in $MnSOD_{cd}$. Indeed, mutation of Gln178 alters the optical signature of the p*Ka* of *E. coli* MnSOD, and changes the value of the p*Ka* from 9.7 to 10 (for Q146L)[57] or 9.0 (for Q146H) [58].

The p*Ka* from pH titration experiments could accommodate the pH dependent activities of $MnSOD_{cd}$ and Fe-sub-$MnSOD_{cd}$. The activity of Fe-sub-$MnSOD_{cd}$ shows pH dependence with a p*K*a of ~7.6 while that of $MnSOD_{cd}$ displays no obvious pH dependence although the overall decreased tendency along with the increased pH. The competition binding of OH^- as the sixth ligand for Fe^{3+} in high pH could repel

substrate and decrease the activity of Fe-sub-$MnSOD_{cd}$. By contrast, the p*Ka* of $MnSOD_{cd}$ corresponds to Tyr64 deprotonation with the increased pH. Although the importing negative charge along with Tyr64 deprotonation would repel substrate, this disadvantage could be offset partly by Gln178's donating hydrogen bond (Gln178 donates stronger hydrogen bond to Tyr64 in $MnSOD_{cd}$). Therefore, the dismutation rate of $MnSOD_{cd}$ reveals intriguing pH independence. However, when pH was increased by a large amount, the activity surely decreased when considering the effect of the lack of proportionation needed protons and the inhibition of protons relaying [59].

(2) Azide as a probe to explore substrate binding for $MnSOD_{cd}$ and Fe-sub-SOD_{cd}

The d^5 electronic configuration of Fe^{3+} *vs* d^4 of Mn^{3+} renders Fe^{3+} owning higher anion affinity than Mn^{3+} based on the Jahn-Teller stabilization[11]. But the azide titrations showed that $MnSOD_{cd}$ anomalously bears higher azide affinity than Fe-sub-$MnSOD_{cd}$. The reasons of which may lie at two aspects: 1. the crystal structure of azide-Fe-sub-$MnSOD_{cd}$ showed that the Thr99 and Arg102 at the outside surface of Fe-sub-$MnSOD_{cd}$ are more prone to grasp azide than those in $MnSOD_{cd}$, which would disfavor azide binding to the inner sphere but lagging at the surface; 2. Tyr64 of SOD_{cd} is proposed to reorient substrate *via* hydrogen bonding interaction with substrate[59]. $MnSOD_{cd}$ should reorganize azide better than Fe-sub-$MnSOD_{cd}$ since Gln178 in $MnSOD_{cd}$ couple more to Tyr64 than Fe-sub-$MnSOD_{cd}$, leading Gln178 propagate more proton density to Tyr64 and stabilizing azide[5]. Therefore, $MnSOD_{cd}$ has lower K_d for binding azide than Fe-sub-$MnSOD_{cd}$.

(3) The reactivities of the Fe and Mn clusters to $O_2^{\cdot-}$ from the proof-of-concept respect

Since the differences of d^5 Fe^{3+} *vs* d^4 Mn^{3+} in the highly similar active sites of $MnSOD_{cd}$/Fe-sub-$MnSOD_{cd}$ are very subtle, the DFT calculation was applied to support their catalytic competencies. We noted that energies of HOMO and LUMO are popular quantum mechanical descriptors[60]. It has been shown that these orbits play a major role in governing many chemical reactions, and are also responsible for charge transfer complexes[61]. Hence, we firstly exploited the FMO theory to explore the electron transfer between superoxide and the metals located in SOD_{cd}, and thus to compare their catalytic potencies. The FMO analysis primarily indicated that the Mn center of $MnSOD_{cd}$ is more prone to dismutate superoxide **(Fig. S4)**.

Furthermore, to dissect their reaction feasibility from the energy respect we performed systematic DFT computational investigations of possible intermediates to be mediated in the reaction cycle of the SOD_{cd}. The spectroscopic titrations indicated that the metals could modulate the SOD catalysis turnover through either modulating the active site p*Ka* or the substrate affinity. The DFT computational investigations were mainly focused on the effects of the intrinsic properties of the active metal sites on the SOD activity. We adopted the associative mechanism for the $O_2^{\cdot-}$ dismutation since a six-coordinate, octahedral intermediate has been observed in Fe- and MnSOD/ N_3^- complex crystal structures[54]. Likewise, spectroscopic studies indicate that the NO adduct to Fe^{2+}SOD was six-coordinate[62]. H_2O or OH^- was considered as the model of the metal-bound solvent molecule since it was proposed as to be an important proton

source[63]. For the second proton, it would be surely transferred to $O_2^{\cdot-}$ by the active site residues, but it is experimentally difficult to determine which residue plays the role of propagating this proton in the reduction step due to the quick reaction process of SOD enzyme. Alternatively, given that superoxide is negatively charged and its protonation must be a corequisite or prerequisite for its reduction, we hypothesized that superoxide anion radical attacks the metal center in its protonation state ($^{\cdot}$OOH) regardless of from which residue it obtains the second proton. The model of $^{\cdot}$OOH is a well simplification from the modeling respect. This treatment means that no charge combination processes need to be modeled, which can be very difficult using the present type of relatively small molecular system. This unified delivery of $O_2^{\cdot-}$ and H^+ is reasonable because: (1) Fe- and $MnSOD_{cd}$ could create a low local pH at the active site to stabilize $O_2^{\cdot-}$, which can be supported by the observations of the high enzyme catalytic rates for Fe- and $MnSOD_{cd}$ under low pH (5.5). Thus the protonation of $O_2^{\cdot-}$ in the active site is feasible. (2) In case the local pH inside the active site is not sufficiently low, this simplification has been subjected to an energy correction using pK_a(OOH) = 4.8. The estimated cost of the protonation for $O_2^{\cdot-}$ at pH = 7.4 is ~3.0 kcal/mol[44] and was added to the energy of the states involving $^{\cdot}$OOH with the aim of referencing them to the true reactants ($O_2^{\cdot-}$ + H^+). The results showed that the reaction ΔG for $MnSOD_{cd}$ was larger than that for Fe-sub-$MnSOD_{cd}$ in both $O_2^{\cdot-}$ oxidation and reduction steps. The free energies of transition states for $MnSOD_{cd}$ are also lower than those of Fe-sub-$MnSOD_{cd}$. Thus $MnSOD_{cd}$ are both thermodynamically and kinetically feasible to disproportionate $O_2^{\cdot-}$, as compared to the Fe-sub-$MnSOD_{cd}$,

which could well backup the experimental activities.

Conclusion

Fe-sub-$MnSOD_{cd}$ was expressed, purified, and characterized by X-ray crystallography, metal analysis, optical and EPR pH titration, azide binding affinity. The pK_a and substrate affinity for the active site determined by spectroscopic titrations indicated that $MnSOD_{cd}$ has a higher affinity to substrate, while Fe-sub-$MnSOD_{cd}$ inclines to bind for OH^-, which accounts for the lower activity of Fe-sub-$MnSOD_{cd}$. The p*K*a of Fe-sub-$MnSOD_{cd}$ is associated with the sixth OH^- binding to Fe^{3+} center, exerting competitive inhibition to its SOD activity, while the p*K*a of $MnSOD_{cd}$ corresponds to the deprotonation of Tyr64. The structural explorations revealed that $MnSOD_{cd}$ orients the substrate into the active site better due to the coupled hydrogen bond of Gln178-Tyr64. The substrate in Fe-sub-$MnSOD_{cd}$ was retarded at the protein surface by hydrogen bond to result in low substrate binding affinity. These findings suggest that SOD_{cd} could modulate the Fe and Mn dependent SOD activity through its active site microenvironment.

Acknowledgement

This work was supported partly by the Natural Science Foundation of China (No. 31270869, 91013001, J1103210), the Ph.D. Program of the Education Ministry of China (20100071110011), Shanghai Synchrotron Radiation Facility (SSRF), and high magnetic field laboratory of Chinese Academy of Science. We would thank Dr. Wei

Tong for his help during EPR measurements.

Conflict of interest

The authors declare that they have no competing financial interests.

Reference

1. D. He, S. Sougioultzis, S. Hagen, J. Liu, S. Keates, A. C. Keates, C. Pothoulakis and J. T. Lamont, *Gastroenterology*, 2002, 122, 1048-1057.
2. A. E. Fisher and D. P. Naughton, *Biomed Pharmacother*, 2005, 59, 158-162.
3. M. A. Farrow, N. M. Chumbler, L. A. Lapierre, J. L. Franklin, S. A. Rutherford, J. R. Goldenring and D. B. Lacy, *Proc Natl Acad Sci U S A*, 2013, 110, 18674-18679.
4. Y. P. Lin, C. J. Kuo, X. Koleci, S. P. McDonough and Y. F. Chang, *J Biol Chem*, 2011, 286, 3957-3969.
5. W. Li, H. Wang, Z. Chen, Q. Ye, Y. Tian, X. Xu, Z. Huang, P. Li and X. Tan, *Chem Commun*, 2014, 50, 584-586.
6. A.-F. Miller, *FEBS Letters*, 2012, 586, 585-595.
7. T. Matsumoto, K. Terauchi, T. Isobe, K. Matsuoka and F. Yamakura, *Biochemistry*, 1991, 30, 3210-3216.
8. D. P. Barondeau, C. J. Kassmann, C. K. Bruns, J. A. Tainer and E. D. Getzoff, *Biochemistry*, 2004, 43, 8038-8047.
9. W. C. Stallings, K. A. Pattridge, R. K. Strong and M. L. Ludwig, *J Biol Chem*, 1984, 259, 10695-10699.
10. B. Meier, A. P. Sehn, C. Michel and M. Saran, *Arch Biochem Biophys*, 1994, 313, 296-303.
11. J. Maliekal, A. Karapetian, C. Vance, E. Yikilmaz, Q. Wu, T. Jackson, T. C. Brunold, T. G. Spiro and A. F. Miller, *J Am Chem Soc*, 2002, 124, 15064-15075.
12. A. F. Miller, *Acc Chem Res*, 2008, 41, 501-510.
13. T. A. Jackson, J. Xie, E. Yikilmaz, A. F. Miller and T. C. Brunold, *J Am Chem Soc*, 2002, 124, 10833-10845.
14. W. C. Stallings, A. L. Metzger, K. A. Pattridge, J. A. Fee and M. L. Ludwig, *Free Radic Res Commun*, 1991, 1, 259-268.
15. Y. Guan, M. J. Hickey, G. E. Borgstahl, R. A. Hallewell, J. R. Lepock, D. O'Connor, Y. Hsieh, H. S. Nick, D. N. Silverman and J. A. Tainer, *Biochemistry*, 1998, 37, 4722-4730.
16. M. M. Whittaker and J. W. Whittaker, *Biochemistry*, 1997, 36, 8923-8931.
17. J. A. Fee and C. Bull, *J Biol Chem*, 1986, 261, 13000-13005.
18. D. L. Tierney, J. A. Fee, M. L. Ludwig and J. E. Penner-Hahn, *Biochemistry*, 1995, 34, 1661-1668.
19. M. Schmidt, *Eur J Biochem*, 1999, 262, 117-127.
20. D. L. Sorkin, D. K. Duong and A. F. Miller, *Biochemistry*, 1997, 36, 8202-8208.

21. R. A. Edwards, M. M. Whittaker, J. W. Whittaker, E. N. Baker and G. B. Jameson, *Biochemistry*, 2001, 40, 4622-4632.
22. C. K. Vance and A. F. Miller, *Biochemistry*, 2001, 40, 13079-13087.
23. F. Yamakura, K. Kobayashi, S. Furukawa and Y. Suzuki, *Free Radical Biology and Medicine*, 2007, 43, 423-430.
24. B. Meier, D. Barra, F. Bossa, L. Calabrese and G. Rotilio, *J Biol Chem*, 1982, 257, 13977-13980.
25. S. Yamano, Y. Sako, N. Nomura and T. Maruyama, *J Biochem*, 1999, 126, 218-225.
26. M. E. Martin, B. R. Byers, M. O. Olson, M. L. Salin, J. E. Arceneaux and C. Tolbert, *J Biol Chem*, 1986, 261, 9361-9367.
27. A. Amano, S. Shizukuishi, H. Tamagawa, K. Iwakura, S. Tsunasawa and A. Tsunemitsu, *J Bacteriol*, 1990, 172, 1457-1463.
28. R. Gabbianelli, A. Battistoni, F. Polizio, M. T. Carri, A. De Martino, B. Meier, A. Desideri and G. Rotilio, *Biochem Biophys Res Commun*, 1995, 216, 841-847.
29. L. C. Tabares, C. Bittel, N. Carrillo, A. Bortolotti and N. Cortez, *J Bacteriol*, 2003, 185, 3223-3227.
30. R. C. Cernat and K. P. Scott, *Anaerobe*, 2012, 18, 298-304.
31. S. M. Poutanen and A. E. Simor, *Canadian Medical Association Journal*, 2004, 171, 51-58.
32. M. M. Bradford, *Anal Biochem*, 1976, 72, 248-254.
33. J. D. Crapo, J. M. McCord and I. Fridovich, *Methods Enzymol*, 1978, 53, 382-393.
34. Z. Otwinowski and W. Minor, *Methods Enzymology*, 1997, 276, 307-326.
35. P. Liu, H. E. Ewis, Y. J. Huang, C. D. Lu, P. C. Tai and I. T. Weber, *Acta Crystallogr Sect F Struct Biol Cryst Commun*, 2007, 63, 1003-1007.
36. P. Emsley and K. Cowtan, *Acta Crystallogr D Biol Crystallogr*, 2004, 60, 2126-2132.
37. A. A. Vagin, R. A. Steiner, A. A. Lebedev, L. Potterton, S. McNicholas, F. Long and G. N. Murshudov, *Acta Crystallogr D Biol Crystallogr*, 2004, 60, 2184-2195.
38. P. D. Adams, P. V. Afonine, G. Bunkoczi, V. B. Chen, I. W. Davis, N. Echols, J. J. Headd, L. W. Hung, G. J. Kapral, R. W. Grosse-Kunstleve, A. J. McCoy, N. W. Moriarty, R. Oeffner, R. J. Read, D. C. Richardson, J. S. Richardson, T. C. Terwilliger and P. H. Zwart, *Acta Crystallogr D Biol Crystallogr*, 2010, 66, 213-221.
39. R. A. Laskowski, M. W. MacArthur, D. S. Moss and J. M. Thornton, *Journal of Applied Crystallography*, 1993, 26, 283-291.
40. M. Pasi, M. Tiberti, A. Arrigoni and E. Papaleo, *J Chem Inf Model*, 2012, 5, 5.
41. G. W. T. M.J. Frisch, H.B. Schlegel, G.E. Scuseria, M.A. Robb, J.R. Cheesman, J.A. Montgomery, Jr., T. Vreven, K.N. Kudin, J.C. Burant, J.M. Millam, S.S. Iyengar, J. Tomasi, V.Barone, B. Mennucci, M. Cossi, G. Scalmani, G.A. Petersson, H. Nakatsuji, M. Hada, M. Ehara, K. Toyota, R. Fukuda, J. Hasegawa, M. Ishoda, T. Nakajima, Y. Honda, O. Kitao, H. Nakai, M. Klene, X. Li, J.E. Knox, H.P. Hratchian, J.B.Cross, C. Adamo, J. Jaramillo, R. Gomperts, R.E. Stratmann, O. Yazyev, A.J. Austin, R. Cammi, C.Pomelli, J. Otcherski, P.Y. Ayala, K. Morokuma, G.A. Voth, P.Salvador, J.J. Danneberg, V.G. Zakrzewski, S. Dapprich, A.D. Daniels, M.C. Strain, O. Farkas, D.K. Malick, A.D. Rabuck, K. Raghavachari, J.B. Foresman, J.V. Ortiz, Q. Cui, A. Baboul, S. Clifford, J. , B. B. S. Cioslowski, G. Liu, A. Liashenko, P. Piskorz, I. Kamaromi, L.R. Martin, D.J. Fox, T. Keith, M.A. Al- Laham, C.Y. Peng, A. Nanaykkara, M. Challacombe, P.M.W. Gill, B. Johnson, W. Chen, M.W. Wong, G. Gonzalez and J. A. Pople, *Gaussian Inc*, 2003.
42. F. Jensen, *Introduction to Computational Chemistry*, John Wiley &Sons, New York, 1999.

43. O. Sackur, *Annalen der Physik*, 1911, 341, 958-980.
44. V. Pelmenschikov and P. E. Siegbahn, *Inorg Chem*, 2005, 44, 3311-3320.
45. K. Fukui, H. Yonezawa and H. Shingu, *J Chem Phys*, 1952, 20, 722-725.
46. J. W. Whittaker, *Biochem Soc Trans*, 2003, 31, 1318-1321.
47. M. M. Whittaker and J. W. Whittaker, *J Biol Inorg Chem*, 2000, 5, 402-408.
48. M. Yang, P. A. Cobine, S. Molik, A. Naranuntarat, R. Lill, D. R. Winge and V. C. Culotta, *Embo J*, 2006, 25, 1775-1783.
49. F. Yamakura, S. Sugio, B. Y. Hiraoka, D. Ohmori and T. Yokota, *Biochemistry*, 2003, 42, 10790-10799.
50. F. Yamakura, K. Kobayashi, H. Ue and M. Konno, *European Journal of Biochemistry*, 1995, 227, 700-706.
51. W.E. Blumberg, *Pergamon Oxford*, 1967, 119-133.
52. A. F. Miller, D. L. Sorkin and K. Padmakumar, *Biochemistry*, 2005, 44, 5969-5981.
53. E. Yikilmaz, J. Porta, L. E. Grove, A. Vahedi-Faridi, Y. Bronshteyn, T. C. Brunold, G. E. Borgstahl and A. F. Miller, *J Am Chem Soc*, 2007, 129, 9927-9940.
54. M. S. Lah, M. M. Dixon, K. A. Pattridge, W. C. Stallings, J. A. Fee and M. L. Ludwig, *Biochemistry*, 1995, 34, 1646-1660.
55. M. Sebaihia, B. W. Wren, P. Mullany, N. F. Fairweather, N. Minton, R. Stabler, N. R. Thomson, A. P. Roberts, A. M. Cerdeno-Tarraga, H. Wang, M. T. Holden, A. Wright, C. Churcher, M. A. Quail, S. Baker, N. Bason, K. Brooks, T. Chillingworth, A. Cronin, P. Davis, L. Dowd, A. Fraser, T. Feltwell, Z. Hance, S. Holroyd, K. Jagels, S. Moule, K. Mungall, C. Price, E. Rabbinowitsch, S. Sharp, M. Simmonds, K. Stevens, L. Unwin, S. Whithead, B. Dupuy, G. Dougan, B. Barrell and J. Parkhill, *Nat Genet*, 2006, 38, 779-786.
56. N. Scheinfeld and K. Biggers, *Curr Opin Investig Drugs*, 2008, 9, 913-924.
57. V. J. Leveque, M. E. Stroupe, J. R. Lepock, D. E. Cabelli, J. A. Tainer, H. S. Nick and D. N. Silverman, *Biochemistry*, 2000, 39, 7131-7137.
58. R. A. Edwards, M. M. Whittaker, J. W. Whittaker, E. N. Baker and G. B. Jameson, *Biochemistry*, 2000, 40, 15-27.
59. A.-F. Miller, *Accounts of Chemical Research*, 2008, 41, 501-510.
60. K. Yamaguchi, M. Shoji, T. Saito, H. Isobe, S. Yamada, S. Nishihara, T. Kawakami, Y. Kitagawa, S. Yamanaka and M. Okumura, *AIP Conference Proceedings*, 2012, 1504, 63-79.
61. K. Yamaguchi, M. Shoji, T. Saito, H. Isobe, S. Nishihara, K. Koizumi, S. Yamada, T. Kawakami, Y. Kitagawa, S. Yamanaka and M. Okumura, *International Journal of Quantum Chemistry*, 2010, 110, 3101-3128.
62. T. A. Jackson, E. Yikilmaz, A. F. Miller and T. C. Brunold, *J Am Chem Soc*, 2003, 125, 8348-8363.
63. L. Rulisek and U. Ryde, *J Phys Chem B*, 2006, 110, 11511-11518.

Tables

Table 1. Summary of data collection and refinement statistics of Azide-Fe-sub-MnSOD$_{cd}$

	Azide-Fe-sub-MnSOD$_{cd}$
Wavelength	0.9792
Space group	$P6_522$
Unit-cell dimensions (Å, °)	a =80.375, b = 80.375, c=250.532 α=β= 90, γ=120
Resolution (Å)	2.1
No.of observations	1217938
No. of unique reflections	29053 (1407)[a]
Completeness (%)	100(100.0)
<I>/(I)	69.5 (9.1)
Redundancy	41.9 (43.2)
R_{sym}[b]	0.094 (0.671)
R_{cryst}[c](%)/R_{free}[d](%)	18.2 / 19.8
RMSD bonds (Å) / angles (°)	0.007 / 0.976
Ramachandran plot, residues in:	
Most favored regions (%)	92.3
Additional allowed regions (%)	6.6
Generously allowed regions (%)	1.1
Disallowed regions (%)	0.0

[a] Numbers in parentheses represent values in the highest resolution shell (Å). [b]R_{sym} = $\Sigma|I_j-\langle I\rangle|/\Sigma I_j$, where I_j is the observed integrated intensity, <I> is the average integrated intensity obtained from multiple measurements, and the summation is over all observed reflections. [c]R_{cryst} =$\Sigma||F_{obs}|-|F_{calc}||/\Sigma|F_{obs}|$, F_{obs} and $F_{calc}$are observed and calculated structure factor amplitudes, respectively. [d]R_{free} calculated with randomly selected reflections (5%)

Table 2. Bond lengths and bond angles at metal active sites and the hydrogen bonds grasping azide in Fe-sub-$MnSOD_{cd}$.

	$MnSOD_{cd}$	Azide-Fe-sub-$MnSOD_{cd}$
A. Coordination bonds (Å)		
M^1-$N^{\varepsilon 2}_{His56}$	2.22 (0.02)	2.16 (0.01)
M-$N^{\varepsilon 2}_{His111}$	2.12 (0.01)	2.23 (0.02)
M-O^2_{Asp193}	1.98 (0.01)	1.91 (0.03)
M-$N^{\varepsilon 2}_{His197}$	2.2 (0.02)	2.19 (0.02)
M-$O_{coordsolv}$	**2.46**(0.04)	**2.23** (0.01)
B. Coordination bond angles (°)		
$N^{\varepsilon 2}_{His197}$-M-$N^{\varepsilon 2}_{His56}$	95.88	101.75
$N^{\varepsilon 2}_{His56}$-M-$O^2_{Asp193}$	83.33	85.12
O^2_{Asp193}-M-$O_{coordsolv}$	80.45	83.51
$O_{coordsolv}$-M-$N^{\varepsilon 2}_{His111}$	95.81	91.47
$N^{\varepsilon 2}_{His111}$-M-$N^{\varepsilon 2}_{His197}$	129.48	126.11
C. Hydrogen bonds (Å)		
Thr99 OG1- N_3^--N3	**3.09**	**2.90**
Arg102 NH1-N_3^--N3	**3.21**	**3.14**

Figures

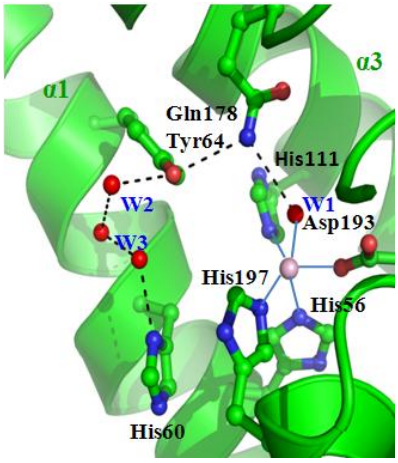

Figure 1. The metal coordination microenvironment of Fe- and $MnSOD_{cd}$.

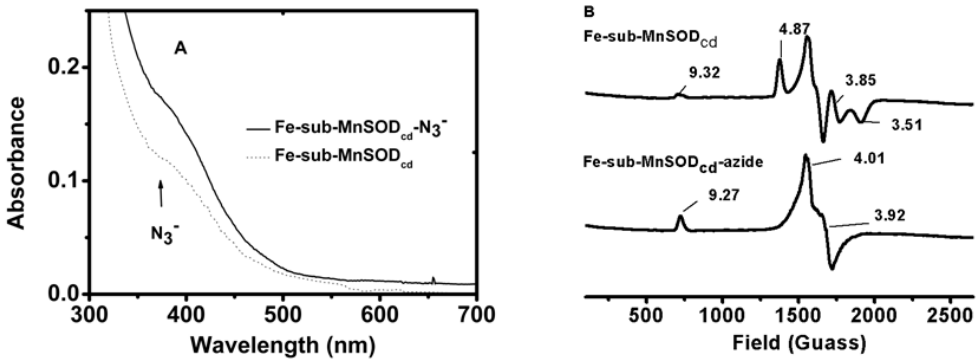

Figure 2. UV/Vis (panel A) and EPR (panel B) spectra of Fe-sub-MnSOD$_{cd}$.

UV/Vis Measurements were performed in buffer containing 100 Mm NaCl, 50 mM potassium phosphate, pH 7.4 and the protein concentration was 10 mg/ml. EPR spectra were collected on a Bruker EMX 300 equipped with an Oxford 900 cytostat, and liquid helium as the coolant, operating at X-band (9.47GHz). The g axis was calibrated at g=2.000 using DPPH.

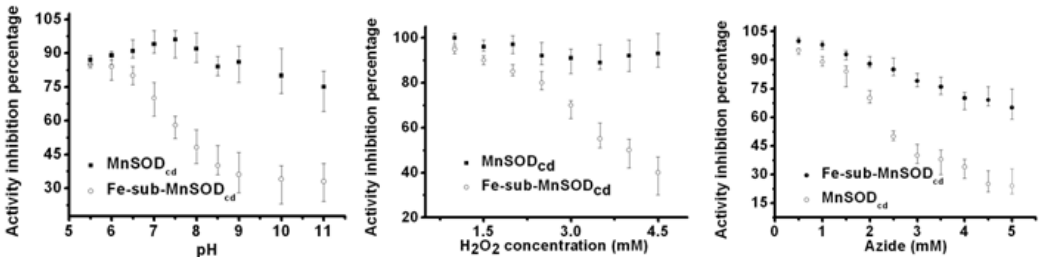

Figure 3. The SOD activity based on XO/cyt *c* assays. Panel A, B and C showed the effects of pH, hydrogen peroxide and azide on the activities of $MnSOD_{cd}$ and Fe-sub-$MnSOD_{cd}$.

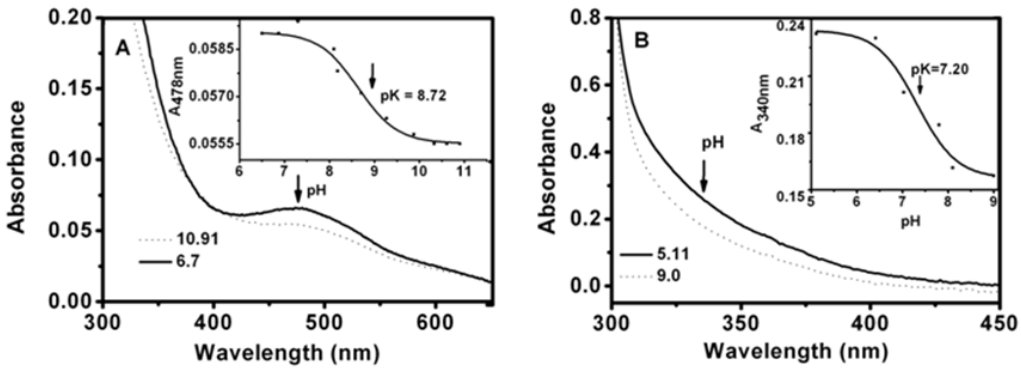

Figure 4. The optical pH titration of $MnSOD_{cd}$ **(Panel A)** and Fe-sub-$MnSOD_{cd}$ **(Panel B).**

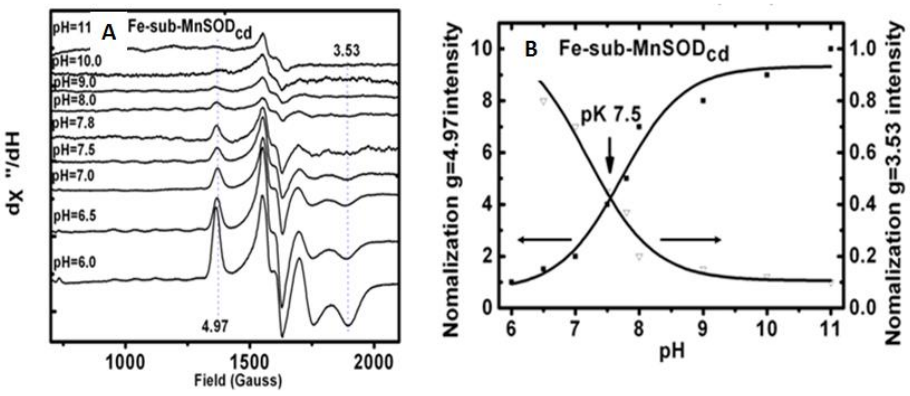

Figure 5. The relevant EPR signals amplitude change along with pH variation of Fe-sub-MnSOD$_{cd}$. **Panel A** shows the different EPR spectra under alterative pH. **Panel B** shows *pK* values of 7.5 for Fe-sub-MnSOD$_{cd}$ by fitting the signals amplitude change as a function of pH values with Henderson-Hasselbalch (n=1) equation.

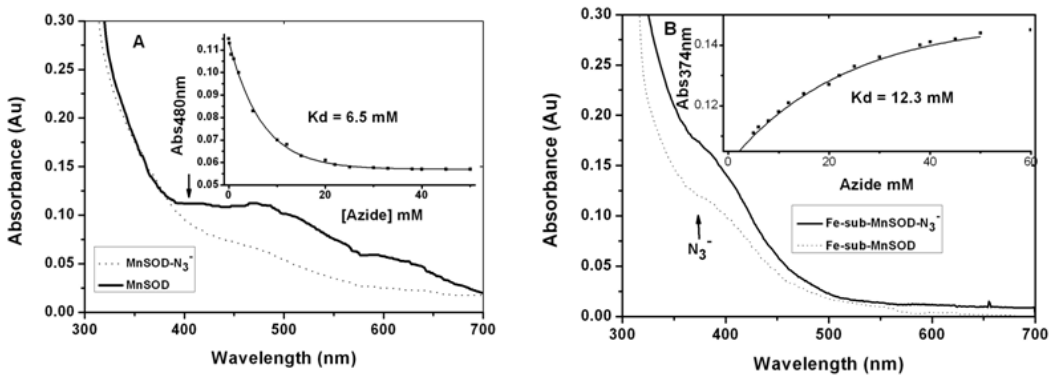

Figure 6. The optical azide titrations of the two SOD_{cd} enzymes. Panel A, B are the spectra of azide binding to $MnSOD_{cd}$ and Fe-sub-$MnSOD_{cd}$. Insets are the fitting curves of the related absorbance change as a function of azide concentration, respectively.

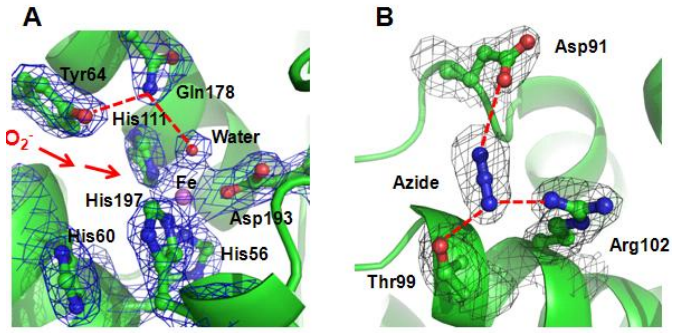

Figure 7. The crystal structure of N_3^--Fe-sub-MnSOD$_{cd}$. Panel A showed the 2Fo-Fc electron density map of the metal coordination microenvironment. **Panel B** showed the 2Fo-Fc electron density map of hydrogen bonds grasping azide.

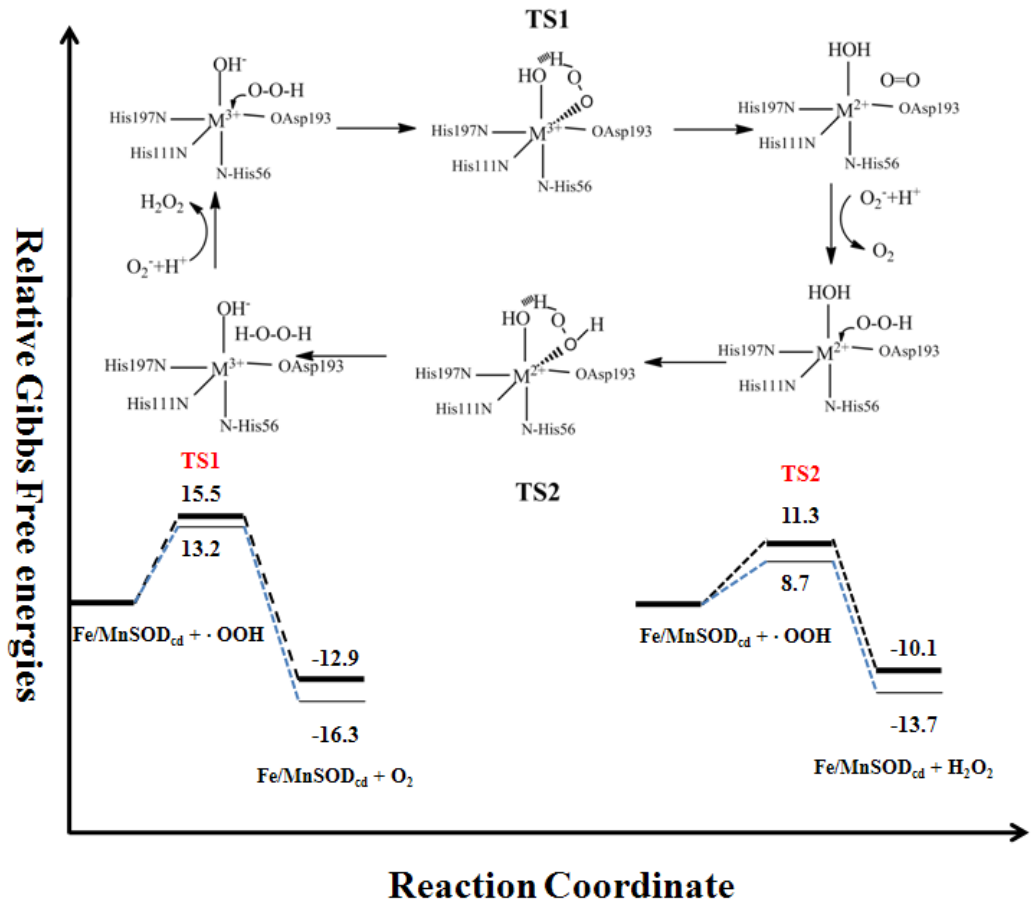

Figure 8. The relative Gibbs energy curves for the superoxide disproportionation reactions were computed at the B3LYP/6-31+(d, p) -6-31+(2d, p) level. The broad lines represent the Gibbs free energies for the reaction catalyzed by Fe-sub-MnSOD$_{cd}$. The thin lines represent the Gibbs free energies for MnSOD$_{cd}$.